PHYSICAL REVIEW E **92**, 041003(R) (2015)

Interface evolution during radial miscible viscous fingering

Jane Y. Y. Chui, Pietro de Anna, and Ruben Juanes*
Massachusetts Institute of Technology, 77 Massachusetts Avenue, Cambridge, Massachusetts 02139, USA
(Received 8 December 2014; revised manuscript received 10 August 2015; published 28 October 2015)

We study experimentally the miscible radial displacement of a more viscous fluid by a less viscous one in a horizontal Hele-Shaw cell. For the range of tested injection rates and viscosity ratios we observe two regimes for the evolution of the fluid-fluid interface. At early times the interface length increases linearly with time, which is typical of the Saffman-Taylor instability for this radial configuration. However, as time increases, the interface growth slows down and scales as $\sim t^{\frac{1}{2}}$, as one expects in a stable displacement, indicating that the overall flow instability has shut down. Surprisingly, the crossover time between these two regimes decreases with increasing injection rate. We propose a theoretical model that is consistent with our experimental results, explains the origin of this second regime, and predicts the scaling of the crossover time with injection rate and the mobility ratio. The key determinant of the observed scalings is the competition between advection and diffusion time scales at the displacement front, suggesting that our analysis can be applied to other interfacial-evolution problems such as the Rayleigh-Bénard-Darcy instability.

DOI: 10.1103/PhysRevE.92.041003 PACS number(s): 47.20.Gv, 47.15.gp, 47.51.+a, 47.54.−r

A large number of natural and industrial flow processes depend on both the degree and the rate of mixing between fluids, such as chemical reactions [1–4], combustion [5], microbial activity [6], and enhanced oil recovery [7]. In such mixing-driven systems, the flow responsible for fluid displacement reflects the heterogeneity of the host medium structure [8–11] or the physical properties of the fluids, such as density [3,12,13] or viscosity [14,15]. Mixing takes place at the fluid-fluid interface and is determined by the combined action of molecular diffusion, which acts to reduce the local concentration gradients, and advection, which controls the interface dynamics [16–21]. Understanding the interface dynamics between two miscible fluids is therefore crucial to explaining and predicting the rate of mixing.

When a less viscous fluid displaces a more viscous one, their interface is deformed and stretched by a hydrodynamical instability known as viscous fingering [15,22,23], and this results in complex interface dynamics [16,17,24]. Much work has focused on characterizing miscible viscous fingering, including laboratory experiments [25–27], numerical simulations [28–32], and linear stability analyses to model the onset and growth of instabilities for rectilinear [33] and radial [34,35] geometries. Other studies have also focused on the effects of anisotropic dispersion [31,33,36], medium heterogeneity [32,37–40], gravity [41–46], chemical reactions [3,47–49], absorption [50], and flow configuration [51–55] on the viscous fingering instability. Despite the extensive work done, the effect of viscous fingering on mixing has only recently been investigated numerically for a rectilinear geometry [14,56]. While the dynamics of the interface between two miscible fluids is crucial to explain and predict the rate of mixing [1,16], a solid understanding of the temporal evolution of the viscously unstable fluid-fluid interface is still missing.

In this Rapid Communication we study experimentally the dynamics of the mixing front for point injection into a circular Hele-Shaw cell initially saturated with a more viscous fluid that is miscible with the injected one (Fig. 1). Recent work has

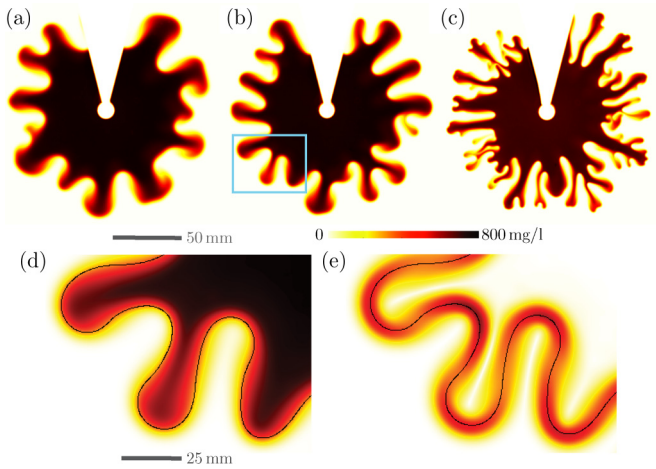

FIG. 1. (Color online) (a)–(c) Concentration fields of the injected fluid displacing a more viscous one (viscosity contrast $M = 10$) at the center of a Hele-Shaw cell at three different flow rates ($Q = 0.004$, 0.008, and 0.02 mL/min, at $t = 5508$, 2416, and 1214 s after the start of injection, respectively). (d), (e) Magnifications of the concentration field and its gradient, respectively. The black line represents the location of the fluid-fluid interface, defined as the locus of the local maxima of the concentration gradient.

reported the experimental observation that pattern evolution for miscible viscous fingering is characterized by rapid growth at early times, followed by slower growth at late times [57]. While diffusion is disregarded in their analysis, here we identify molecular diffusion as the mechanism responsible for the shutdown of the instability at late times. In our experiments, the long-enough times (or small-enough strain rates) imply that diffusion plays a major role in the evolution of the interface, and that Korteweg stresses and nonequilibrium surface tension effects do not [56,58–66]. As the unstable front grows in fingerlike structures [Figs. 1(a)–1(c)], molecular diffusion smears the local concentration gradients at the interface by mixing the two fluids.

The system is divided into three regions that evolve in time: the inner region occupied only by the displacing fluid, the

*juanes@mit.edu

outer region occupied only by the displaced fluid (that initially was saturating the Hele-Shaw cell), and the region where both fluids coexist, the *mixing zone* Γ. Given the large aspect ratio of the Hele-Shaw geometry, we adopt an approximation of the fluid-fluid interface—which in reality is a three-dimensional (3D) surface—as a two-dimensional (2D) curve. We define Γ as the region where, locally, the fraction χ of invading fluid is $0 < \chi < 1$. Incompressible advection conserves volume fluid elements without changing their concentration; the physical mechanism responsible for the local variation of χ is molecular diffusion.

Since the fluids used in our experiments are miscible, the transition between the two fluids is diffuse. We define the fluid-fluid interface γ as the set of points where $\nabla\chi$ is locally maximum, which corresponds to where the mixing rate is also locally maximum [14,19]. Here, we focus on understanding the mechanisms controlling the temporal evolution of the length Σ of the interface γ, and we propose an effective model able to describe and predict its dynamics.

To quantify the topology of γ and the dynamics of Σ in this radial configuration, we developed an experimental technique to directly measure the temporal evolution of the concentration field c of a tracer dissolved in the injected fluid. The experimental setup is a Hele-Shaw cell composed of two horizontal transparent glass disks of radius $R = 111$ mm separated by a thin gap $b = 0.1$ mm. A hole of radius $R_i = 0.8$ mm at the center of each glass plate is used to inject fluid at a constant flow rate Q, which we impose with a syringe pump. The cell has separate injection ports for the defending (more viscous) and invading (less viscous) fluids to ensure that no mixing occurs prior to entering the Hele-Shaw cell. The cell is initially saturated with a transparent water-glycerol mixture of viscosity μ_2, and through the inlet on the top plate we inject a solution of water and a fluorescent tracer (fluorescein sodium salt of concentration $c_0 = 800$ mg/L) of viscosity $\mu_1 = 0.9$ cP. We performed experiments by varying systematically the flow rate Q in the range 0.004 mL/min $\leqslant Q \leqslant$ 0.02 mL/min and the mobility ratio $M = \mu_2/\mu_1$ (by changing μ_2) in the range $1 \leqslant M \leqslant 25$. The fluid-fluid displacement patterns are imaged from the top of the cell with a scientific complementary metal-oxide semiconductor (CMOS) camera at a frame rate of 5 Hz, at a resolution of 90 μm per pixel.

We use standard fluorescent microscopy to measure the local concentration field of the transported tracer [20,67]: The local concentration of the fluorescent tracer is related to the amount of photons emitted by the tracer via a calibration procedure, which resulted in a linear relation between light intensity and tracer concentration over three decades.

We measure γ and its length Σ from the concentration gradient. The interface γ is defined as the ridges (local maxima) of the concentration gradient ∇c, which are computed with a Hessian-based Voronoi tesselation algorithm applied to the concentration field [Figs. 1(d) and 1(e)].

In Fig. 2 we show the temporal evolution of the interface length Σ for five different injection rates and a mobility ratio $M = 10$. We make two main observations. First, for all injection rates Q we distinguish two regimes for the temporal scaling of Σ. At early times, the interface length increases almost linearly with time, as perhaps can be expected from the Saffman-Taylor instability in this radial configuration [33]. In

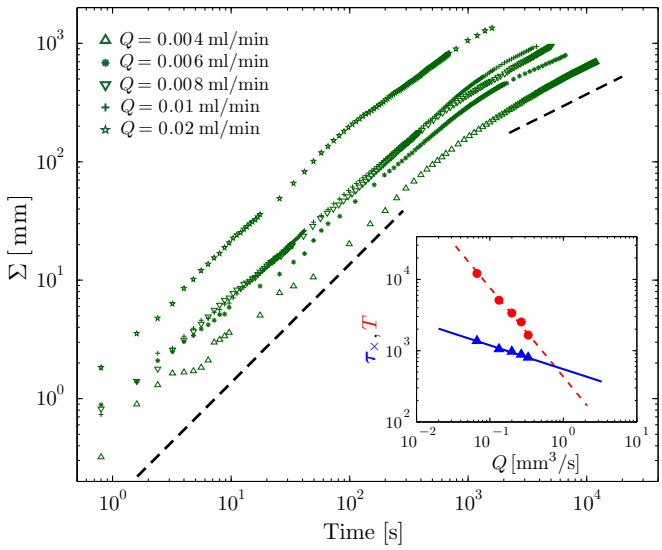

FIG. 2. (Color online) Time evolution of the interface ($M = 10$). There exist two regimes, the first of rapid growth due to active viscous fingering, and the second of slower growth that corresponds to radial expansion of a frozen finger pattern. The crossover into the second regime occurs at earlier times for faster injection rates. Inset: Crossover time $\tau_\times$ between regimes (blue triangles) and total experimental time T (red circles) for the $M = 10$ experiments. The estimate of $\tau_\times$ is obtained from the theoretical model developed below. T decreases with increasing injection rates faster than $\tau_\times$—an indication of the decreasing duration (and eventual absence) of the second regime for increasing injection rates.

all cases, at a given time, the interface growth slows down and begins to evolve as $\Sigma \sim t^{1/2}$. This means that the overall flow instability is no longer active and the fluid-fluid displacement is merely expanding radially with a frozen fingering pattern. The transition between the two regimes is prolonged in time. However, we define the crossover time $\tau_\times$ as the time after which no instability should be observed—that is, as the "end" of the transition between the two regimes. The second key observation is that the crossover time $\tau_\times$ between these two regimes decreases with increasing injection rate Q (Fig. 2 inset). This result is counterintuitive, since a stronger flow injection leads to a more vigorous instability [14].

Understanding the underlying mechanisms that control interface growth is paramount for the study of mixing and chemical reactions in this configuration [3,49,68]. Here, we propose a theoretical model to explain these two observations and predict both the crossover time $\tau_\times$ between the two regimes, and the scaling of the length of the interface $\Sigma_\times$ at this time with Q and M. We then use the results of our analysis to rescale the data in Fig. 2 and collapse them onto a single curve.

Crossover time $\tau_\times$. The observed change in scaling for the temporal evolution of interface length Σ suggests the existence of conditional stability. We hypothesize that this conditional stability occurs as a consequence of molecular diffusion mixing the two fluids along the diffuse interfacial region. To test this hypothesis, we define the characteristic diffusion time over the length l as $\tau_{\text{diff}} = l^2/D_m$, and the characteristic advection time of the average front displacement

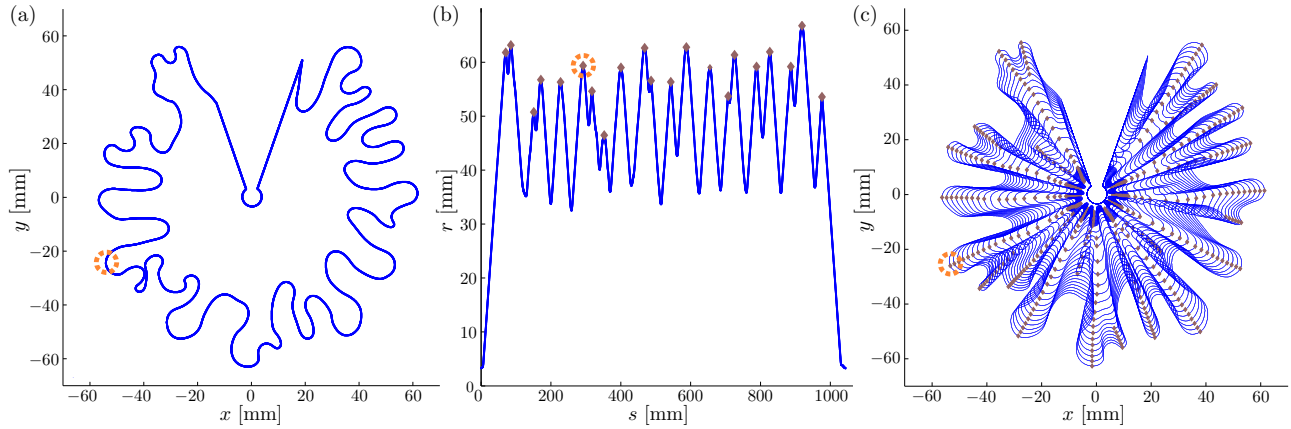

FIG. 3. (Color online) Determination of finger-tip positions and number of fingers. (a) At each time step, the Cartesian coordinates (x,y) of the interface γ are converted into a radial-curvilinear coordinate system (r,s), where r is the radial distance from the injection point (center of the image) and s is the distance along the interface γ. For each value of s, a single value of r is defined, and thus the pattern is "unravelled." (b) We define the finger tips as the local maxima (brown diamonds) of the curve $r(s)$, which allows for a robust determination of the number of fingers. (c) The finger-tip positions can be mapped onto the (x,y)-coordinate system, and tracked as a function of time. The orange circle in (a)–(c) indicates the same finger through the steps of image processing used to determine the number of fingers.

over the same length as $\tau_{\text{adv}} = l/v_f$, where v_f is the average front velocity and D_m is the diffusion coefficient. For a constant injection rate Q, the volume of fluid injected after a time t is $Qt = \pi r_f^2 b$, where r_f is the effective radius of fluid displacement. Therefore, we propose the straightforward scaling of the average front velocity to be $v_f = dr_f/dt = \sqrt{[Q/(4\pi bt)]}$.

For a given length scale l along the interface, as long as the advective time is smaller than the diffusive time, the fluids across that length l at the front remain unmixed, and the instability is sustained. Thus, we estimate the characteristic time $\tau(l)$ for mixing over a distance l along the interface by imposing $\tau_{\text{adv}} = \tau_{\text{diff}}$, which gives $\tau(l) = (Ql^2)/(4\pi bD_m^2)$.

We define the critical length scale l_c as the size of the dominant perturbation produced by the front instability, for a given initial viscosity contrast M and injection rate Q. Once the two fluids across this length l_c are mixed by diffusion, we expect the transition to take place. We define $l_c = 2\pi R_i/(2n_f)$, where R_i is the radius of the injection port, and n_f is the observed number of fingers (see Fig. 3 for a detailed description of the determination of the number of fingers). Experimentally, we find that $n_f \sim Q^{2/3}M^{1/2}$ (Fig. 4). Thus, $l_c \sim Q^{-2/3}M^{-1/2}$, and inserting this result into the expression for $\tau(l)$, the crossover time scales as

$$\tau_\times \sim Q^{-1/3}M^{-1}. \tag{1}$$

This result is in agreement with our observations: The crossover to the regime of radial expansion happens earlier for higher injection rates (Fig. 4 inset).

We now compare our scalings for l_c derived experimentally with the results of linear stability analysis for this flow configuration [33]: The state of the system is represented by the sum of a stable solution (corresponding to $M = 1$) and small perturbations that are decomposed into Fourier modes with wave number n. It has been shown that the instability amplifies those perturbations and the growth rate σ of their modes scales as

$$\sigma = \frac{\log M\sqrt{\text{Pe}}}{\sqrt{\pi}}\left(1 - \frac{\sqrt{\text{Pe}}}{n}\right) - \frac{n^2}{\text{Pe}}, \tag{2}$$

where the Péclet number is defined as $\text{Pe} = Q/(bD_m)$ [33], so for constant gap thickness b, $\text{Pe} \sim Q$. The perturbation growth rate σ is negative for low and high values of the wave number n, which means that perturbations (fingers) that are too wide or too narrow are not amplified. The most unstable wave number

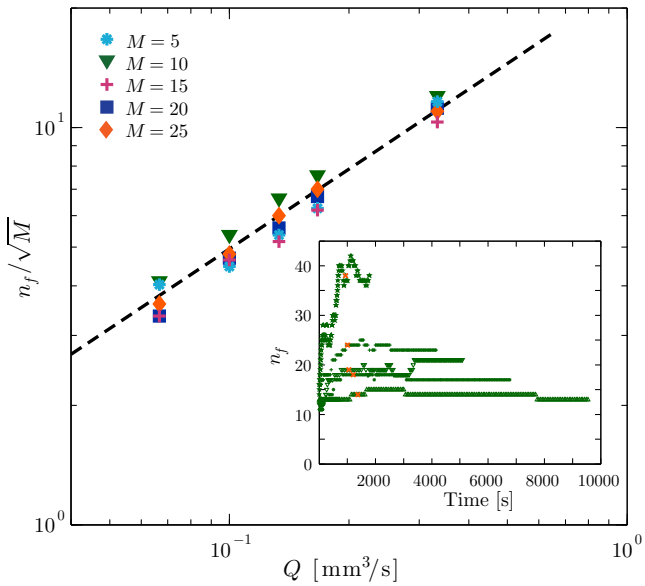

FIG. 4. (Color online) Experimental measurements of number of fingers n_f as a function of injection rate Q for all mobility ratios M tested. The number of fingers scales as $Q^{2/3}M^{1/2}$ (the dashed line denotes a $Q^{2/3}$ scaling). Inset: Evolution of n_f with time for $M = 10$ and five different values of Q. For all injection rates, n_f first increases as a result of tip splitting, but then stabilizes around the crossover time (marked with a red cross for each experiment).

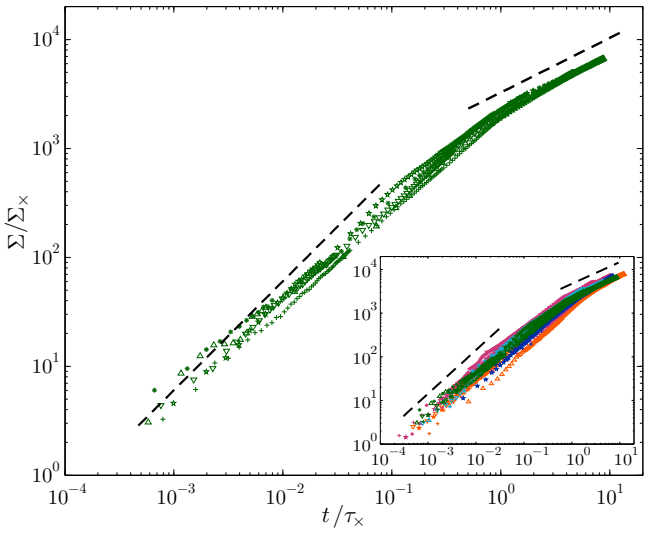

FIG. 5. (Color online) Rescaled interface length vs rescaled time, for $M = 10$. By rescaling each data set with the crossover time [Eq. (1)] and the interface length expected at this crossover time [Eq. (3)], the data sets collapse onto a single curve, and the crossover into the second regime occurs at $t/\tau_\times \approx 1$. Inset: The same rescaling applied to all the experimental data: $M = 5, 10, 15, 20, 25$ (different colors) for the five different injection rates (different symbols).

$n_{\max}$ [the maximum of Eq. (2); Fig. 4 inset] corresponds to the fastest growing, and therefore dominant, perturbation wavelength of the system. From Eq. (2), the scaling of the most unstable wave number $n_{\max}$ with Q is found to be $Q^{2/3}$ and with M to be $(\log M)^{1/3}$. The scaling with injection rate (and therefore with Péclet number) from experimental observations is in agreement with the linear stability analysis. This is not the case, however, for the scaling with viscosity ratio—something that can be attributed to the fact that the experiments are conducted well into the nonlinear regime.

The interface length Σ *at* $\tau_\times$. We estimate the total interface length Σ as the product of the number of fingers n_f and the average finger length l_f, $\Sigma \sim n_f l_f$. As discussed above, the number of fingers n_f scales as $Q^{2/3} M^{1/2}$.

The average finger length at the crossover time is obtained by integrating the average tip velocity u_f in time. We estimate u_f as the growth rate σ of the most unstable wave number, $n = n_{\max}$, from Eq. (2). Substituting in the observed scalings $n_f \sim n_{\max}$, and assuming that the average tip velocity is constant in time, $u_f(t) \sim \log M \, \mathrm{Pe}^{1/2}$, the length of the fingers at the crossover time scales as $l_f(t = \tau_\times) \sim \log M \, \mathrm{Pe}^{1/2} \, \tau_\times$. Substituting this into the expression for interface length at the crossover time, we get an overall scaling of $\Sigma(t = \tau_\times) \sim M^{1/2} \log M \, Q^\alpha$, where α is the sum of the exponents for the number and average length of fingers: $\alpha = 2/3 + 1/2 - 1/3 = 5/6$. Thus, at the crossover time $\tau_\times$, the interface length scales as

$$\Sigma_\times \sim n_f l_f \sim M^{1/2} \log M \, Q^{5/6}. \tag{3}$$

These findings provide a general picture of the dynamics of the interface length Σ across the range of experimental conditions investigated. By rescaling time with the crossover time $\tau_\times$ [Eq. (1)] and the interface length by $\Sigma_\times$ [Eq. (3)], we find that the different curves of Σ vs t collapse onto a single curve (Fig. 5). For $t/\tau_\times < 1$, the interface length grows linearly in the absence of fluid mixing at such early time, in analogy with the Saffman-Taylor instability. For $t/\tau_\times > 1$, the interface length grows as $t^{1/2}$, characteristic of proportional growth (radial expansion with a frozen finger pattern), indicating that the viscous fingering instability has shut down. The transition from $\sim t$ to $\sim t^{1/2}$ scaling of interface length is apparent once the appropriate length and time scales have been found—an indication that the proposed behavior emerges more clearly from the entire data set than from individual experiments. The same results hold for all the other mobility ratios investigated (Fig. 5 inset).

Our experimental observations and scaling analysis elucidate the underlying mechanisms responsible for the evolution of interface length in miscible viscous fingering. These results are crucial to understanding, describing, and predicting the mixing dynamics [69]. The universality of our arguments—balance between advection and diffusion at the displacement front—suggests that our proposed framework can be applied to other front geometries or other types of hydrodynamic instability in miscible flows, such as Rayleigh-Bénard, and density-driven convection in porous media [4,12,70,71].

Beyond their intrinsic interest for the understanding of a fundamental hydrodynamic instability [14,15,51,56,57], our results suggest that the shutdown of the viscous fingering instability in a radial configuration could be important for predicting the effectiveness of enhanced oil recovery by miscible flooding [7,72], where well-to-well flows are dominated by radial displacements during the early stages of the flood [52,53,73].

[1] Z. Neufeld and E. Hernández-García, *Chemical and Biological Processes in Fluid Flows: A Dynamical Systems Approach* (Imperial College Press, London, 2010).
[2] G. Károlyi, Phys. Rev. E **71**, 031915 (2005).
[3] A. De Wit, Phys. Rev. Lett. **87**, 054502 (2001).
[4] V. Loodts, C. Thomas, L. Rongy, and A. De Wit, Phys. Rev. Lett. **113**, 114501 (2014).
[5] D. Martínez-Ruiz, J. Urzay, A. L. Sánchez, A. Liñán, and F. A. Williams, J. Fluid Mech. **734**, 387 (2013).
[6] W. M. Durham, E. Climent, and R. Stocker, Phys. Rev. Lett. **106**, 238102 (2011).
[7] L. W. Lake, *Enhanced Oil Recovery* (Prentice-Hall, Englewood Cliffs, NJ, 1989).
[8] P. de Anna, T. Le Borgne, M. Dentz, A. M. Tartakovsky, D. Bolster, and P. Davy, Phys. Rev. Lett. **110**, 184502 (2013).
[9] T. Le Borgne, M. Dentz, and J. Carrera, Phys. Rev. Lett. **101**, 090601 (2008).
[10] B. Bijeljic, P. Mostaghimi, and M. J. Blunt, Phys. Rev. Lett. **107**, 204502 (2011).
[11] P. K. Kang, M. Dentz, and R. Juanes, Phys. Rev. E **83**, 030101(R) (2011).

[12] J. J. Hidalgo, J. Fe, L. Cueto-Felgueroso, and R. Juanes, Phys. Rev. Lett. **109**, 264503 (2012).
[13] C. W. MacMinn and R. Juanes, Geophys. Res. Lett. **40**, 2017 (2013).
[14] B. Jha, L. Cueto-Felgueroso, and R. Juanes, Phys. Rev. Lett. **106**, 194502 (2011).
[15] G. M. Homsy, Annu. Rev. Fluid Mech. **19**, 271 (1987).
[16] J. Ottino, *The Kinematics of Mixing: Stretching, Chaos, and Transport*, Cambridge Texts in Applied Mathematics (Cambridge University Press, Cambridge, U.K., 1989).
[17] T. Tél, A. de Moura, C. Grebogi, and G. Károlyi, Phys. Rep. **413**, 91 (2005).
[18] E. Villermaux, C. R. Mec. **340**, 933 (2012).
[19] T. Le Borgne, M. Dentz, and E. Villermaux, Phys. Rev. Lett. **110**, 204501 (2013).
[20] P. de Anna, J. Jiménez, H. Tabuteau, R. Turuban, T. Le Borgne, M. Derrien, and Y. Méheust, Environ. Sci. Technol. **48**, 508 (2014).
[21] P. de Anna, M. Dentz, A. Tartakovsky, and T. Le Borgne, Geophys. Res. Lett. **41**, 4586 (2014).
[22] J. D. Chen, J. Fluid Mech. **201**, 223 (1989).
[23] P. Petitjeans and T. Maxworthy, J. Fluid Mech. **326**, 37 (1996).
[24] J. Jiménez and C. Martel, Phys. Fluids A **3**, 1261 (1991).
[25] A. R. Kopf-Sill and G. M. Homsy, Phys. Fluids **31**, 242 (1988).
[26] J. C. Bacri, N. Rakotomalala, D. Salin, and R. Wouméni, Phys. Fluids A **4**, 1611 (1992).
[27] P. Petitjeans, C. Y. Chen, E. Meiburg, and T. Maxworthy, Phys. Fluids **11**, 1705 (1999).
[28] M. A. Christie and D. J. Bond, SPE Reserv. Eng. **2**, 514 (1987).
[29] C. T. Tan and G. M. Homsy, Phys. Fluids **31**, 1330 (1988).
[30] M. A. Christie, SPE Reserv. Eng. **4**, 297 (1989).
[31] W. B. Zimmerman and G. M. Homsy, Phys. Fluids A **3**, 1859 (1991).
[32] W. B. Zimmerman and G. M. Homsy, Phys. Fluids A **4**, 1901 (1992).
[33] C. T. Tan and G. M. Homsy, Phys. Fluids **29**, 3549 (1986).
[34] C. T. Tan and G. M. Homsy, Phys. Fluids **30**, 1239 (1987).
[35] A. Riaz, C. Pankiewitz, and E. Meiburg, Phys. Fluids **16**, 3592 (2004).
[36] Y. Yortsos and M. Zeybek, Phys. Fluids **31**, 3511 (1988).
[37] C. T. Tan and G. M. Homsy, Phys. Fluids A **4**, 1099 (1992).
[38] H. A. Tchelepi, F. M. Orr, Jr., N. Rakotomalala, D. Salin, and R. Wouméni, Phys. Fluids A **5**, 1558 (1993).
[39] A. De Wit and G. M. Homsy, J. Chem. Phys. **107**, 9609 (1997).
[40] A. De Wit and G. M. Homsy, J. Chem. Phys. **107**, 9619 (1997).
[41] H. A. Tchelepi and F. M. Orr, Jr., SPE Reserv. Eng. **9**, 266 (1994).
[42] O. Manickam and G. M. Homsy, J. Fluid Mech. **288**, 75 (1995).
[43] E. Lajeunesse, J. Martin, N. Rakotomalala, and D. Salin, Phys. Rev. Lett. **79**, 5254 (1997).
[44] M. Ruith and E. Meiburg, J. Fluid Mech. **420**, 225 (2000).
[45] J. Fernandez, P. Kurowski, P. Petitjeans, and E. Meiburg, J. Fluid Mech. **451**, 239 (2002).
[46] A. Riaz and E. Meiburg, J. Fluid Mech. **494**, 95 (2003).
[47] J. Fernandez and G. M. Homsy, J. Fluid Mech. **480**, 267 (2003).
[48] A. De Wit and G. M. Homsy, J. Chem. Phys. **110**, 8663 (1999).
[49] Y. Nagatsu, K. Matsuda, Y. Kato, and Y. Tada, J. Fluid Mech. **571**, 475 (2007).
[50] M. Mishra, M. Martin, and A. De Wit, Phys. Fluids **19**, 073101 (2007).
[51] L. Paterson, Phys. Fluids **28**, 26 (1985).
[52] H. R. Zhang, K. S. Sorbie, and N. B. Tsibuklis, Chem. Eng. Sci. **52**, 37 (1997).
[53] C. Y. Chen and E. Meiburg, J. Fluid Mech. **371**, 233 (1998).
[54] D. Pritchard, J. Fluid Mech. **508**, 133 (2004).
[55] C.-Y. Chen, C.-W. Huang, H. Gadêlha, and J. A. Miranda, Phys. Rev. E **78**, 016306 (2008).
[56] B. Jha, L. Cueto-Felgueroso, and R. Juanes, Phys. Rev. Lett. **111**, 144501 (2013).
[57] I. Bischofberger, R. Ramachandran, and S. R. Nagel, Nat. Commun. **5**, 5265 (2014).
[58] H. T. Davis, in *Proceedings of the Symposium on Numerical Simulation in Oil Recovery* (Springer, New York, 1988), pp. 105–110.
[59] H. H. Hu and D. D. Joseph, Z. Angew. Math. Phys. **43**, 626 (1992).
[60] D. D. Joseph, A. Huang, and H. H. Hu, Physica D **97**, 104 (1996).
[61] C.-Y. Chen and E. Meiburg, J. Fluid Mech. **326**, 57 (1996).
[62] C.-Y. Chen, L. Wang, and E. Meiburg, Phys. Fluids **13**, 2447 (2001).
[63] C.-Y. Chen and E. Meiburg, Phys. Fluids **14**, 2447 (2002).
[64] S. Swernath, B. Malengier, and S. Pushpavanam, Chem. Eng. Sci. **65**, 2284 (2010).
[65] D. Truzzolillo, S. Mora, C. Dupas, and L. Cipelletti, Phys. Rev. Lett. **112**, 128303 (2014).
[66] S. Pramanik and M. Mishra, Europhys. Lett. **109**, 64001 (2015).
[67] P. Bunton, B. Dice, J. A. Pojman, A. De Wit, and F. Brau, Phys. Fluids **26**, 114106 (2014).
[68] Y. Nagatsu, Y. Ishii, Y. Tada, and A. De Wit, Phys. Rev. Lett. **113**, 024502 (2014).
[69] J. Y. Y. Chui, P. de Anna, and R. Juanes (unpublished).
[70] S. Backhaus, K. Turitsyn, and R. E. Ecke, Phys. Rev. Lett. **106**, 104501 (2011).
[71] D. R. Hewitt, J. A. Neufeld, and J. R. Lister, Phys. Rev. Lett. **108**, 224503 (2012).
[72] F. I. Stalkup, Jr., *Miscible Displacement*, SPE Monograph Series Vol. 8 (Society of Petroleum Engineers, Dallas, TX, 1983).
[73] C. Y. Chen and E. Meiburg, J. Fluid Mech. **371**, 269 (1998).